Mathematical modeling and harmonic analysis of SISFCL

Mathematical modelling and harmonic analysis of SISFCL

SCHOLARONE™
Manuscripts

Mathematical modelling and harmonic analysis of SISFCL

INTRODUCTION

In present times, the size of power system networks has increased by many folds to meet the growing power demand of the modern world. As a consequence of the continuous growth of power generation, the power system networks approach or even exceed their limits with respect to their short circuit withstand capability (Morandi, 2013). The necessity of changing the protective equipment in order to operate at higher fault level has increased further with the inclusion of distributed generators and increasing power of the feeder loads (Duggan, 2006; Morandi, 2013; Fajoni, et al., 2015). Countering the problem of excessive short circuit current has become an important issue for the power system operators both at transmission as well as distribution levels. Reliance on traditional means of remedying the adverse effects of fault current to satisfy reliable and safe power distribution, especially in the context of rapidly growing electricity demand, is not sustainable. Therefore, the use of advanced and innovative current limiting devices is necessary for future developments of the modern power system. Interest in SISFCL is gaining momentum nowadays owing to its fast response to a fault and quick subsequent recovery. In recent years, it is gradually finding its way into both power system transmission and distribution applications (Moriconi, et al., 2011; Xiao, et al., 2011; Kazemia & Lehtonenb, 2013).

High temperature superconductors such as BSCCO, YBCO etc. require an efficient cooling to sustain the superconducting state. The HTS coil is required to be maintained in the cryogenic system (Hong, et al., 2014; Xiao, et al., 2011). The open cryogenic system, where there is a continuous refilling of the liquid nitrogen is favoured for its economic aspects.

The SISFCL utilizes the ability to change the magnetic state of the ferromagnetic core from saturation to unsaturation to provide low impedance during normal operation and high impedance during fault. Needless to say, this change in magnetic state is dependent significantly on the relation between flux density (B) and magnetic field intensity (H) of the core. Previous mathematical models (He, et al., 2014; Li, et al., 2015) describing the working of the SISFCL, have considered a simple B-H curve. However, this relationship could be more realistically addressed when hysteresis is considered in its place. This paper presents a mathematical model of the SISFCL considering the Jiles Atherton hysteresis model (Jiles, et al., 1992; Iványi, 1997). Moreover different hysteresis loops have been utilized and the transient responses of the limiter are compared to investigate its performance with variation in hysteresis characteristics. Simulations are carried out using both MATLAB and ANSYS MAXWELL software.

WORKING PRINCIPLE

The structure of the SISFCL consists of two ferromagnetic cores biased by a common superconducting coil (Fig. 1) carrying DC current. The opposite limbs of the cores support the windings which are in series with the circuit. The AC coils are wound in opposition to one another. During normal operation the DC biasing current is adjusted such that both the cores remain in saturation. The flux produced by the AC current during normal operation is small and cause insignificant change in saturation of the core. Since during this state the permeability μ is very low, the effective impedance of the device is very small. Hence the device offers negligible impedance to the circuit under normal operation. During fault the AC current increases drastically, producing high value of AC ampere-turns which is now comparable to the DC ampere-turns. The core where the AC flux opposes the DC flux reduces the effective flux distribution and the core comes out of saturation and reaches the unsaturation zone. The other core reaches a more saturated state as the AC flux adds to the DC biasing flux. The situation persists during one half-cycle and it reverses in the other half cycles. As the permeability in the unsaturated state is high the effective value of the impedance of the

device increases significantly and fault current is thus suppressed. The reaction time of the device for limiting the fault current and its subsequent recovery is almost instantaneous as the operation solely depends on the change of the magnetic state of the core.
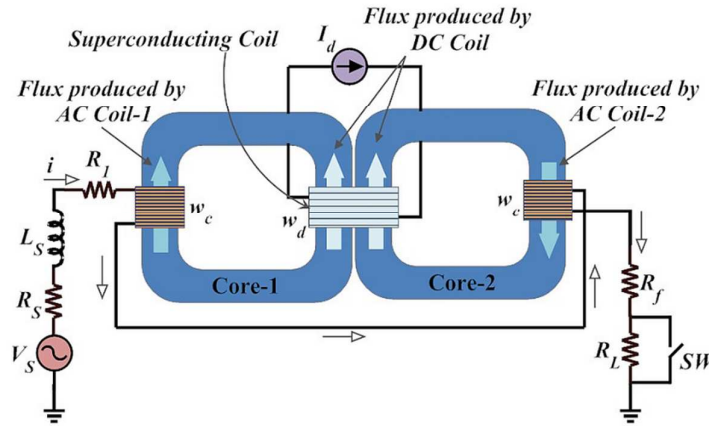

Fig. 1. Schematic diagram of SISFCL

JILES-ATHERTON'S HYSTERESIS MODEL

Since the change of the magnetic state of the core plays a very important role in operation of the device, inclusion of the effects of hysteresis in the model will give a more accurate result. Of the various mathematical models describing hysteresis, the Preisach's model and the Jiles-Atherton's (J-A) hysteresis model are more popular. For the current analysis the Jiles- Atherton model is considered. The basis of the J-A model is the anhysteretic magnetization (M_{an}) curve which represents the ideal lossless magnetization of a material. The mathematical representation is given by the equation considering a as the shaping coefficient,

$$M_{an} = M_{sat}(coth\left(\frac{H_e}{a}\right) - \frac{a}{H_e})$$ (1)

The saturation magnetisation is denoted by M_{sat} and H_e is the effective field intensity. According to the model, the magnetization of the material is the sum of the reversible (M_{rev}) and the irreversible (M_{irr}) components. The irreversible component is describe as,

$$\frac{dM_{irr}}{dH} = \frac{M_{an} - M_{irr}}{k\delta - \alpha(M_{an} - M_{irr})}$$ (2)

Where $\delta = sign(dH/dt)$ is a directional parameter, $+1$ for $dH/dt > 0$ and -1 for $dH/dt < 0$, k is a parameter that defines the pinning site density of domain walls and is the scaling factor for H_e. The reversible component is considered as the difference between the anhysteretic and the irreversible component of the magnetization, given by the equation,

$$M_{rev} = c(M_{an} - M_{irr})$$ (3)

Where c is a domain flexing parameter, defining the amount of reversible magnetization due to wall bowing and reversal rotation, included in the magnetization process. Considering the above equations and rearranging the terms, the J-A model is described as,

$$\frac{dM}{dH} = \frac{(1-c)\dfrac{M_{an} - M}{sign(\frac{dH}{dt})k(1-c) - \alpha(M_{an} - M)} + c\dfrac{dM_{an}}{dH_e}}{1 - \alpha c \dfrac{dM_{an}}{dH_e}}$$ (4)

The above equation describing the hysteresis is utilized in the mathematical model of the SISFCL.

MATHEMATICAL MODEL

The mathematical model is developed taking the schematic diagram (Fig.1) of the circuit in consideration. The SISFCL is shown to be in series in between the voltage source (V_s) and the load (R_L) along with a fault resistance R_f. The fault is simulated by bypassing the load R_L. The source resistance and inductance is denoted by R_s and L_s respectively, whereas R_1 representing the total coil resistance. The variables w_d and w_c represent the number of turns of the DC and AC current carrying windings respectively. The mean magnetic path of each core and the DC biasing current is represented by l and I_d respectively. Following Ampere's Law, it can be written,

$$w_d I_d - w_c i = H_1 l \tag{5}$$
$$w_d I_d + w_c i = H_2 l \tag{6}$$

The induced voltage drop across two coils (u_1 and u_2) are obtained after subsequent calculation and are expressed as,

$$u_1 = -\mu_0 w_c A \frac{dH_1}{dt}(1 + \frac{dM_1}{dH_1}) = L\frac{di}{dt}(1 + \frac{dM_1}{dH_1}) \tag{7}$$

$$u_2 = -(-\mu_0 w_c A \frac{dH_2}{dt}(1 + \frac{dM_2}{dH_2})) = L\frac{di}{dt}(1 + \frac{dM_2}{dH_2}) \tag{8}$$

Where $L = \frac{\mu_0 w_c^2 A}{l}$. Now following Kirchhoff's Law,

$$V_s(t) = u_1 + u_2 + u_R + u_L = u_1 + u_2 + i(R_s + R_1 + R_f + R_L) + L_s \frac{di}{dt} \tag{9}$$

Where u_R is the voltage drop across total resistance and u_L is the voltage drop across the source inductance. Hence after substitution and rearrangement the differential equation describing the working of the SISFCL is obtained. The developed equation is as follows,

$$\frac{di}{dt} = \frac{V_s(t) - i(R_s + R_1 + R_f + R_L)}{L(2 + \frac{dM_1}{dH_1} + \frac{dM_2}{dH_2}) + L_s} \tag{10}$$

SIMULATION

As the change in the magnetic state is vital for the performance of the device, it is obvious that different core materials with varying hysteresis characteristics will have significant effect in the responses of the device. In order to explore this variation, three hysteresis characteristics are employed (Jiles, et al., 1992) in the simulation (Table I). The comparative plots of the characteristics are shown in Fig. 2.
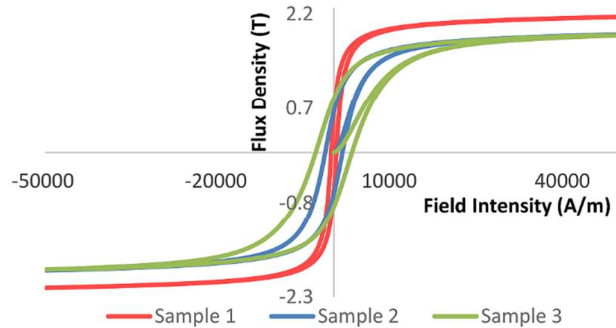
Fig. 2. Hysteresis plot of the sample cores

MATLAB simulation

Simulations are executed using the parameter values shown in Table II at 50 Hz, the fault being simulated at 0.02 sec. Although the simulation is carried for 0.14s, in order to provide a better comparison with FEM output, discussed in the next section, the responses are shown for 0.06s except for the B vs. H plot.

The transient response of the current waveforms, shown in Fig. 3, demonstrates the effect of the variation of hysteresis loops on the current limiting capability of the FCL and the prospective fault condition. It is observed that the presence of FCL do not affect the normal current as it presents a low impedance close to twice the value of an air core inductor (Moscrop, 2013). The simulation results reveal that the fault current has been suppressed in presence of SISFCL. It may also be noted that wider is the hysteresis loop of the core, lesser is the fault suppression, although the waveform remains identical during normal operation. The small mmfs developed in the AC coils are unable to bring the core to unsaturated state overcoming the DC biasing. As a result, the core remains in the saturated state, providing negligible permeability (μ). Hence the current in the normal condition remains unaltered even with the variation of hysteresis characteristics of the core.
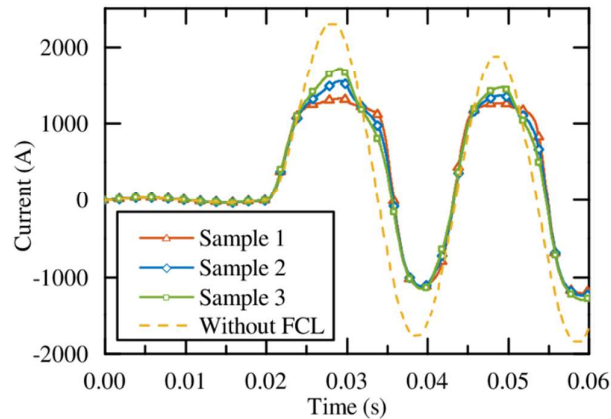

Fig. 3. Comparative circuit current plot

But during a fault instant, the high value of mmf developed in the AC coil brings the core to unsaturated condition. As different hysteresis loops present different values of permeability for a given field intensity, the impedance offered by the limiter during fault varies. Moreover, the shape of the hysteresis loop plays an important role in developing the shape of the suppressed current as the rate of change of flux density varies against the same change in field intensity for different hysteresis loops. There has also been a noticeable phase shift in the suppressed current from the prospective current signifying the increase in reactance of the limiter. It can be also observed that change in the suppressed current is more profound in the positive half of the cycle. This happens due to the presence of dc offset component during the fault event. The higher magnitude of the positive half of the current brings the core more in the unsaturated zone than the negative half. This phenomenon disappears after 3 to 4 cycles as the dc offset decreases to zero.

Fig. 4 shows the voltage across the FCL under normal and fault conditions. During the normal operation, the voltage across the limiter is negligible, indicating a low impedance of the device. Changes in the hysteresis characteristics have insignificant effect on the voltage across the SISFCL during the normal operation. It is only during the fault instances that the effect of the core characteristics can be perceived. The FCL with the highest suppression has the highest voltage across the limiter and vice versa. It is observed that the voltage waveform during the fault attains a characteristic double peak pattern (Zhang & Dougal, 2012; Xiao, et al., 2011). This double peak occurs when the current decreases to zero completing the positive half of the cycle and enters the

negative half. During this period, the unsaturated core moves to saturation reducing the voltage magnitude momentarily. With the commencement of the next half of the cycle the other core becomes unsaturated and the voltage magnitude increases thus creating the double peak. The presence of the dc offset component also has its effect on the waveform making the double peaks uneven. Equal sized peaks can be realized only after decay of the dc offset.
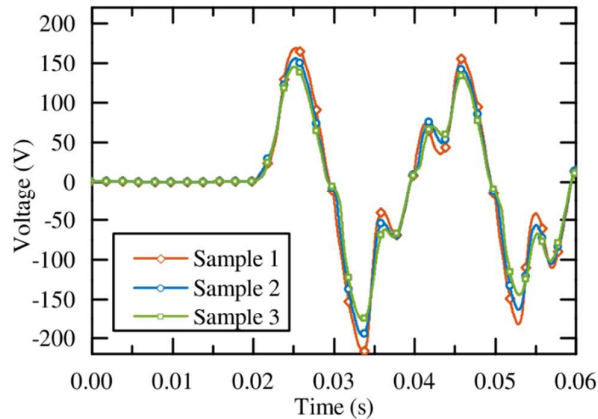

Fig. 4. Comparative plot of the voltage across SISFCL

The voltage across the DC bias coils (Fig. 5) shows that the value remains very small in the normal condition and increases significantly following a fault. The reason for this behaviour is that in normal operation, the DC m.m.f. is very high compared to the AC m.m.f. and hence there is a very small change in the flux density inside the DC limb. However during fault the AC m.m.f. increases significantly so that its interaction with the DC m.m.f. produces a significant change in the flux density. The voltage across the DC biasing coil is seen to be maximum when fault current suppression is highest. The development of a high voltage across the DC biasing coil is of great concern as high induced voltage is capable of damaging the DC source. Various methods have been put forward in mitigating this issue (Cui, et al., 2014).
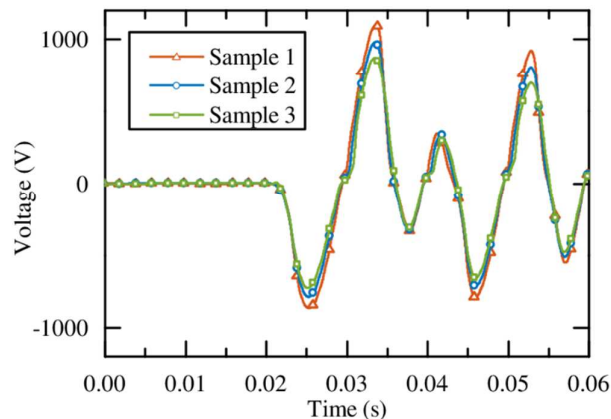

Fig. 5. Comparative plot of the voltage across the DC bias coil of the SISFCL

Fig. 6 and Fig. 7 show the flux density versus field intensity plot in both core 1 and core 2, respectively, for the entire period of 0.14s. During normal operation, the field intensity of the DC bias remains at about 18 kA/m. But during fault, the value of flux density reduces following the hysteresis pattern of the core.
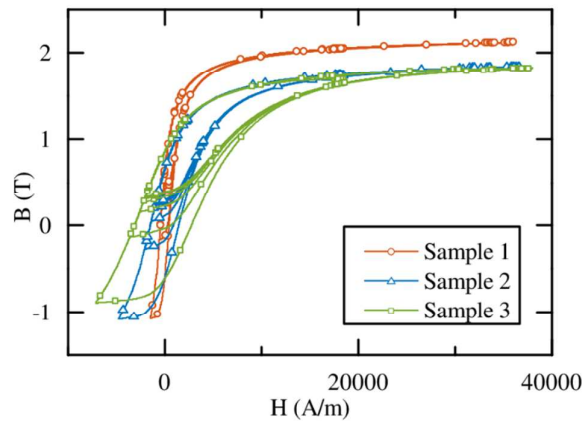
Fig. 6. Comparative plot of the B-H characteristics for Core 1

As there is a marked difference in the slope of the plots in the unsaturated region, the impedance imposed by the limiter differs to provide different limiting. It is also observed that since the initial cycles after fault occurrence have a higher current magnitude in the positive half of the cycle than the negative half, the flux density reaches a more negative value in core 1 as it gets unsaturated in the positive half of the cycle. With the disappearance of the dc offset, the flux densities of both the cores change in a similar manner.
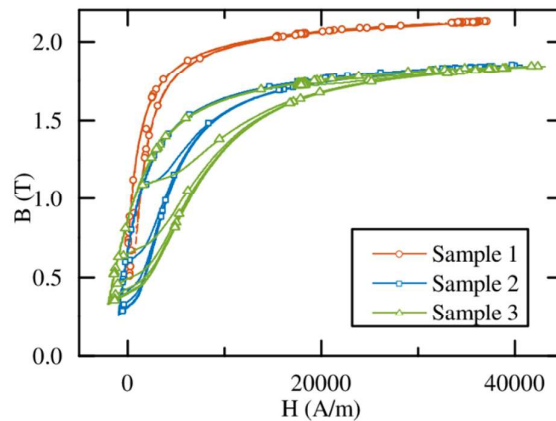

Fig. 7. Comparative plot of the B-H characteristics for Core 2

FEM simulation

The finite element method has been a popular choice for simulations concerning electromagnetics. It has become an important tool for research and has produced results that has successfully reached close agreement to the experimental outcome (Kurt, et al., 2014; Kurt, et al., 2016; Uzun & Kurt, 2013; Uzun, et al., 2015).As the response of the SISFCL is very much dependent on the change in the magnetic state, simulation of the limiter using FEM becomes essential. Moreover, the mathematical models of the SISFCL developed have all been based on the approximation of a constant flux density distribution throughout the entire core. Hence for a proper investigation of this electromagnetic device the FEM analysis is required. For these simulations, the Transient Solver of Ansoft Maxwell 2D is employed. The later versions of the software allows hysteresis to be included in the core loss property of the material. It requires the B-H curve data and the corresponding values of the coercive force and remanence to develop the hysteresis loop. It needs to be mentioned here that ANSYS Maxwell always

consider the magnetization as isotropic magnetization if the hysteresis model is included. The hysteresis data is fed into the material properties of the core and hence, three independent simulations were run. For the simulations, the parameter values were kept the same as in Table II and it is run for 0.06s with a fault occurring at 0.02s. The simulation time is reduced to just 3 cycles to shorten the computation time.

The field analyses shown in Fig. 8 show the normal and faulted states of the FCL. The normal condition shown in Fig. 8(a) illustrates deep saturation in the entire core region. Fig. 8(b) demonstrates the faulted state where the left side core comes out of saturation due to high fault current. The right side core reaches a more saturated zone as the flux in the AC winding adds to the DC winding flux. This condition persists for one half of the cycle while the phenomenon is just reversed in the next half cycle. Core sample 1 is considered for the field distribution plot.
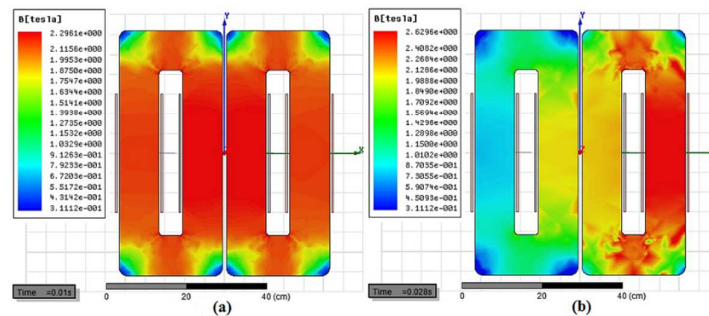

Fig. 8. Plot of flux distribution in the cores (a) Normal condition (b) Fault condition

The comparative current plot shown in Fig. 9 produces a similar result as in the case of the previous simulation. The presence of the DC offset at the fault occurrence has produced a variation in current magnitude in the first half of the cycle whereas in the negative half cycle the difference becomes very small. The core sample with narrower hysteresis loop offers more suppression than the one with wider hysteresis loop.
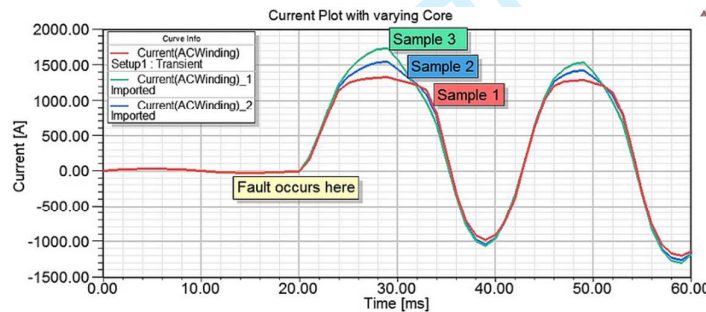

Fig. 9. Comparative plot of circuit current

The plots of the voltage across the limiter is shown in Fig. 10. As it is observed from the simulation shown in the previous section, the voltage is desirably very low in the normal condition. With the fault occurrence, the magnitude of the voltage increases significantly. Although the FEM simulation shows a similar result compared to the MATLAB simulation, the double peak is less profound in the FEM solution. It has been previously discussed that the double peak occurs with the change of core magnetic state. But unlike in the mathematical model, the flux density distribution is not uniform throughout the core and the rate of change of the flux distribution is lesser, causing a shallow dip in the voltage waveform.
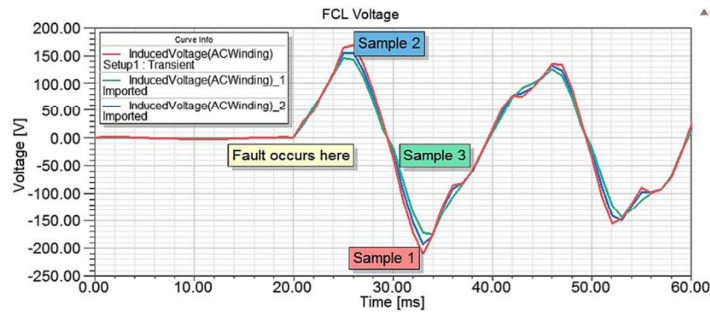
Fig. 10. Comparative plot of voltage across the SISFCL

The voltage across DC bias coils (Fig. 11) have also produced similar results to the previous simulation although the voltage peaks after fault occurrence, adjacent to zero crossing, is found to be a little less in the FEM simulation. While the MATLAB model is built on an approximation of constant flux throughout the core, the FEM simulation reveals a difference in the flux values in the AC and the DC core limb. This difference in the flux density can be attributed for voltage shortcomings.
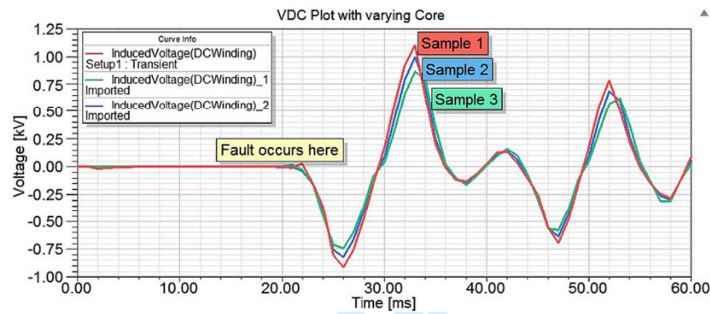

Fig. 11. Comparative plot of voltage across DC bias coil of the SISFCL

The above discussions have revealed a reasonable closeness to the results obtained in both the methods. The minor discrepancies between the results are accredited to the approximations made in the mathematical model. Nevertheless, a fair agreement of the outputs undoubtedly supports the validity of the mathematical model of the SISFCL.

HARMONIC ANALYSIS

The current responses of the SISFCL have not only shown that the degree of suppression changes with the core material but also that the shape of the responses indicates a varied level of harmonics being injected in the system. Hence to study the variation a harmonic analysis is necessary. This paper demonstrates harmonic analysis of the limiter current waveform using the Fast Fourier Transform (FFT) and Continuous Wavelet Transform (CWT).

Fast Fourier Transform

FFT has been a popular method for harmonic analysis. The FFT analysis of the current waveform was performed in MATLAB. The signal was split into two parts, separating the normal and the fault signal, which were analyzed separately. The comparative FFT plot of the circuit current in the normal condition is given in Fig. 12. It can be seen that for all 3 sample cores, there are no other harmonic contents in the signal aside from the fundamental. However, in the comparative FFT plot of the faulted circuit current, as given in Fig. 13, presence of higher order harmonics can be observed. Moreover the sample core with the narrower hysteresis loop is found to inject a higher magnitude of harmonics in the faulted condition and the core with the wider hysteresis loop is found to inject the least magnitude of harmonics in the faulted situation.
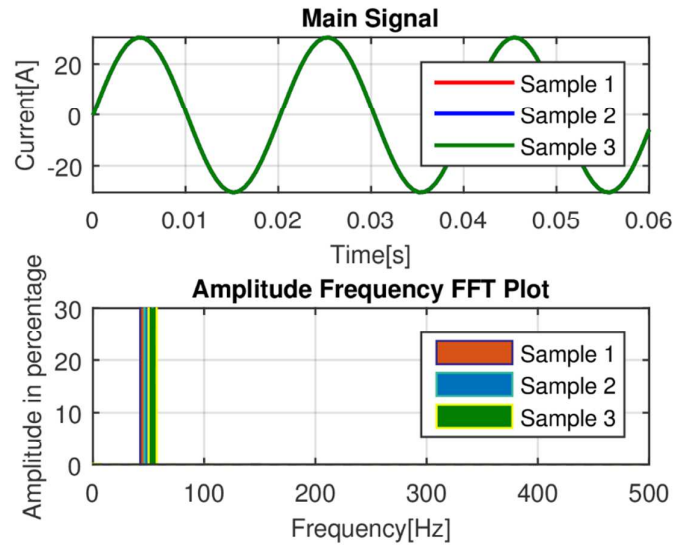
Main Signal

Amplitude Frequency FFT Plot

Fig. 12. FFT of the current signal during normal operation
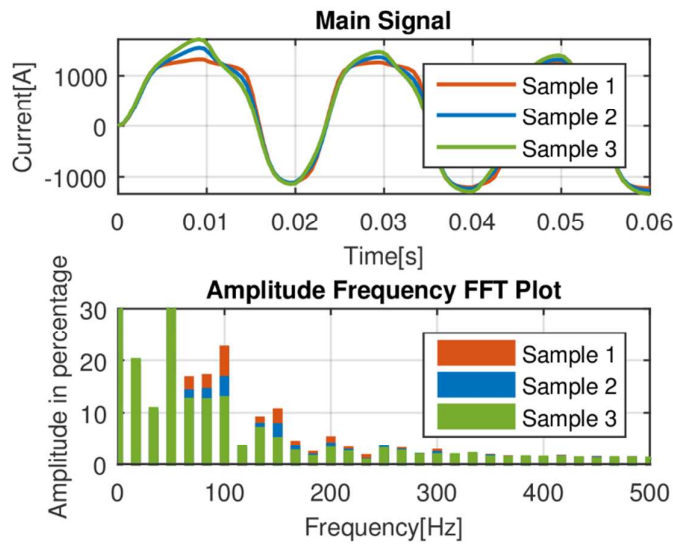
Main Signal

Amplitude Frequency FFT Plot

Fig. 13. FFT of the current signal during fault condition

Continuous Wavelet Transform

As the interharmonic estimation obtained from FFT is erroneous due to spectral leakage, the Continuous Wavelet Transform (CWT) is used for a more accurate time and frequency resolution of the current signal. For any given signal $f(t)$, the continuous wavelet transform is defined as,

$$W(a,b) = \int_t f(t) \frac{1}{\sqrt{|a|}} \Psi\left(\frac{t-b}{a}\right) dt \tag{11}$$

And the wavelet is given as,

$$\Psi_{a,b}(t) = \int_t \frac{1}{\sqrt{|a|}} \Psi\left(\frac{t-b}{a}\right) dt \tag{12}$$

Where a is the dilation or scaling parameter and b is the translation or location parameter. Similar to the FFT analysis, the CWT has been performed on the current signal after isolating the normal and fault signal. For the present analysis the Morlet Wavelet is taken as the mother wavelet. Fig. 14 shows the normal current with its CWT. As expected, there are no harmonics present other than the

fundamental. The CWT analysis of the circuit current in the faulted condition, given in Fig. 15, shows the presence of higher order harmonics. Similar to the results obtained from FFT, it is observed that the sample core with the narrower hysteresis loop contains the highest magnitude of harmonics and the core with the wider hysteresis loop contains the least. Thus the results obtained from CWT analysis support the results obtained from FFT analysis.
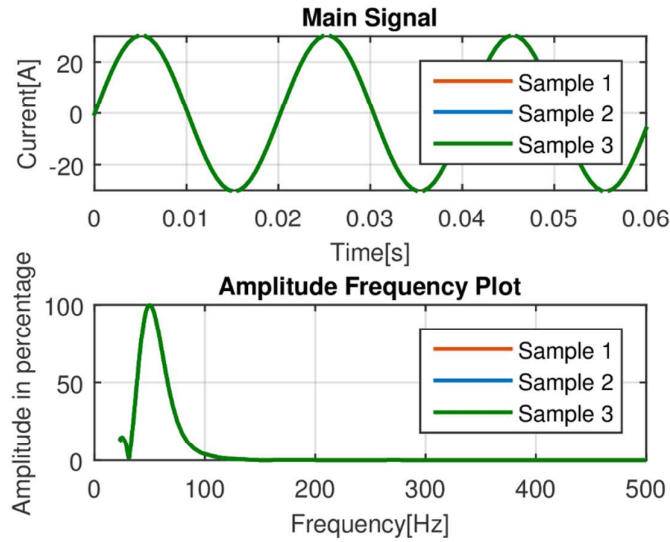

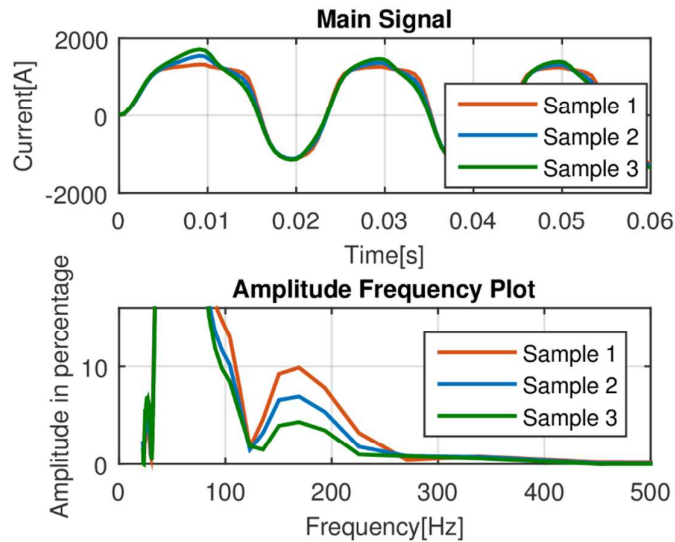Fig. 14. CWT of the current signal during normal condition

Fig. 15. CWT of the current signal during fault condition

Conclusion

This paper successfully illustrates the development of a mathematical model of the SISFCL. As the operation of the device relies solely on the change of the magnetic state of saturation and unsaturation of the ferromagnetic core, the effects of magnetic hysteresis is included using the Jiles-Atherton model of hysteresis. Moreover, to analyze the operation of the SISFCL in further detail, three cores of different hysteresis loops were considered. The model was numerically solved and the solutions were obtained using MATLAB. It was shown that the fault current suppression considering the core with a narrower hysteresis loop will provide a better suppression than a core with wider hysteresis loop. It is

observed that the voltage across the limiter under fault condition is highest when the fault current suppression is maximum. The voltage across the DC coil reveals the fact that better the suppression, higher is the voltage appearing across the DC coil. Hence a wider hysteresis curve helps in reducing the induced voltage developed across DC bias circuit. In support of the numerical analysis, FEM analyses with the same parameters were performed using Ansoft Maxwell 2D software. The flux distributions across the core were shown for both normal and faulted conditions. The solutions obtained in the FEM simulation are in close agreement to the responses obtained from the numerical method. Comparisons were made on the harmonic content of the current signal using both FFT and CWT (using Morlet Wavelet). The harmonic analysis has demonstrated negligible harmonic content in the current signal during normal condition for all core samples. However during fault condition, the presence of higher order harmonics is observed. The percentage amplitude of higher order harmonics in the fault current is observed to be more in the core with narrower hysteresis loop.

REFERENCE

Cui, J. et al., 2014. Study on field suppression unit in dc excitation system for saturated iron-core superconducting fault current limiter. *Applied Superconductivity, IEEE Transactions on,* 24(5), pp. 1-4.

Duggan, P. M., 2006. Integration issues for fault current limiters and other technologiesa utility perspective. s.l., IEEE, pp. 1-3.

Fajoni, F., Ruppert, E., Baldan, C. & Shigue, C., 2015. Study of superconducting fault current limiter using saturated magnetic core. Journal of Superconductivity and Novel Magnetism, 28(2), p. 685–690.

He, Y. et al., 2014. Control system modeling and simulation of superconducting current limiter with saturated iron core controlled by dc bias current. *Applied Superconductivity, IEEE Transactions on,* 24(5), pp. 1-6.

Hong, H. et al., 2014. Design, Fabrication, and Operation of the Cryogenic System for a 220 kV/300 MVA Saturated Iron-Core Superconducting Fault Current Limiter. IEEE Transactions on Applied Superconductivity, 24(5), pp. 1-4.

Iványi, A., 1997. Hysteresis Models in Electromagnetic Computation. Budapest: Akadémiai Kiadó.

Jiles, D., Thoelke, J. & Devine, M., 1992. Numerical determination of hysteresis parameters for the modelling of magnetic properties using the theory of ferromagnetic hysteresis. *Magnetics, IEEE Transactions on,* 28(1), pp. 27-35.

Kazemia, S. & Lehtonenb, M., 2013. Impact of smart subtransmission level fault current mitigation solutions on service reliability. Electric Power Systems Research, Volume 6, pp. 9-15.

Kurt, E., Gör, H. & Demirtaş, M., 2014. Theoretical and experimental analyses of a single phase permanent magnet generator (PMG) with multiple cores having axial and radial directed fluxes. Energy Conversion and Management, Volume 77, pp. 163-172.

Kurt, E., Gör, H. & Döner, U., 2016. Electromagnetic design of a new axial and radial flux generator with the rotor back-irons. International Journal of Hydrogen Energy, 41(17), pp. 7019-7026.

Li, B., Guo, F., Wang, J. & Li, C., 2015. Electromagnetic transient analysis of the saturated iron-core superconductor fault current limiter. *Applied Superconductivity, IEEE Transactions on,* 25(3), pp. 1-5.

Morandi, A., 2013. State of the art of superconducting fault current limiters and their application to the electric power system. *Physica C: Superconductivity,* Volume 484, pp. 242-247.

Moriconi, F. et al., 2011. Development and deployment of saturated-core fault current limiters in distribution and transmission substations. *Applied Superconductivity, IEEE Transactions on,* 21(3), pp. 1288-1293.

Moscrop, J., 2013. Experimental analysis of the magnetic flux characteristics of saturated core fault current limiters. *Magnetics, IEEE Transactions on,* 49(2), pp. 874-882.

Uzun, Y. & Kurt, E., 2013. The effect of periodic magnetic force on a piezoelectric energy harvester. Sensors and Actuators A: Physical, Volume 192, pp. 58-68.

Uzun, Y., Kurt, E. & Kurt, H. H., 2015. Explorations of displacement and velocity nonlinearities and their effects to power of a magnetically-excited piezoelectric pendulum. Sensors and Actuators A: Physical, Volume 224, pp. 119-130.

Xiao, H. et al., 2011. Analysis of transient overvoltage in 220 kv saturated core hts fcl. *Magnetics, IEEE Transactions on,* 47(10), pp. 2620-2623.

Zhang, Y. & Dougal, R., 2012. State of the art of fault current limiters and their applications in smart grid. *Power and Energy Society General Meeting*, July, pp. 1-6.

Table I: J-A constants of the sample core

	M_s	c	k	α	a
Sample 1	$1.7{\times}10^6$	0.1	500	1×10^{-3}	1000
Sample 2	$1.5{\times}10^6$	0.14	1800	1.4×10^{-3}	1800
Sample 3	$1.5{\times}10^6$	0.1	4000	1×10^{-3}	2000

Table II: System parameters in the simulation model

Name	Symbol	Value
Source Voltage	V_s	220V
Source Resistance	R_s	6.56mΩ
Source Inductance	L_s	0.215mH
Sum total of Cabling Resistances and the Resistance of the two AC coils	R_1	27.84mΩ
Load Resistance	R_L	7.2Ω
Fault Resistance	R_f	67.9mΩ
Effective cross-section Area of each limb	A	0.01254m^2
Mean Magnetic Path length	l	1.36m
Number of DC windings	w_d	102
Number of AC windings	w_c	20
DC bias current	I_d	240A